

February 18, 2019

Unbiased analysis of CLEO data at NLO and pion distribution amplitude

A. P. Bakulev¹, S. V. Mikhailov²

*Joint Institute for Nuclear Research, Bogoliubov Lab. of Theoretical Physics,
141980, Moscow Region, Dubna, Russia*

N. G. Stefanis³

*Institut für Theoretische Physik II, Ruhr-Universität Bochum,
D-44780 Bochum, Germany*

Abstract

We discuss different QCD approaches to calculate the form factor $F^{\gamma^*\gamma\pi}(Q^2)$ of the $\gamma^*\gamma \rightarrow \pi^0$ transition giving preference to the light-cone QCD sum rules (LCSR) approach as being the most adequate. In this context we revise the previous analysis of the CLEO experimental data on $F^{\gamma^*\gamma\pi}(Q^2)$ by Schmedding and Yakovlev. Special attention is paid to the sensitivity of the results to the (strong radiative) α_s -corrections and to the value of the twist-four coupling δ^2 . We present a full analysis of the CLEO data at the NLO level of LCSRs, focusing particular attention to the extraction of the relevant parameters to determine the pion distribution amplitude, i.e., the Gegenbauer coefficients a_2 , a_4 . Our analysis confirms our previous results and also the main findings of Schmedding and Yakovlev: both the asymptotic, as well as the Chernyak–Zhitnitsky pion distribution amplitudes are completely excluded by the CLEO data. A novelty of our approach is to use the CLEO data as a means of determining the value of the QCD vacuum non-locality parameter $\lambda_q^2 = \langle \bar{q}D^2q \rangle / \langle \bar{q}q \rangle = 0.4 \text{ GeV}^2$, which specifies the average virtuality of the vacuum quarks.

PACS: 11.10.Hi,12.38.Bx,12.38.Lg,13.40.Gp

Keywords: Transition form factor, Pion distribution amplitude, QCD sum rules, Factorization, Renormalization group evolution

¹E-mail: bakulev@thsun1.jinr.ru

²E-mail: mikhs@thsun1.jinr.ru

³E-mail: stefanis@tp2.ruhr-uni-bochum.de

1 Introduction

Recently, the CLEO collaboration [1] has measured the $\gamma^*\gamma \rightarrow \pi^0$ form factor $F^{\gamma^*\gamma\pi}(Q^2)$ with high precision. This data has been processed by Schmedding and Yakovlev (SY) [2] using light-cone QCD sum rules (LCSR), taking also into account the perturbative QCD contributions in the next-to-leading order (NLO) approximation. In this way SY obtained useful constraints on the shape of the pion distribution amplitude (DA) in terms of confidence regions for the Gegenbauer coefficients a_2 and a_4 , the latter being the projection coefficients of the pion DA on the corresponding eigenfunctions. Note that SY have extended to the NLO the LCSR approach suggested before by Khodjamirian [3] for the leading order (LO) light-cone sum rule method.

The present analysis gives further support to the claim, expressed by the above mentioned authors, that LCSRs provide the most appropriate basis in describing the form factor of the $\gamma^*\gamma \rightarrow \pi^0$ transition. This is intimately connected with peculiarities of real-photon processes in QCD [4, 3]. But the method of the CLEO data processing, adopted in [2], seems to be not quite complete from our point of view. We think that an optimal analysis should take into account the correct ERBL evolution of the pion DA to the scale Q_{exp}^2 of the process (the latter not to be fixed at some average point, $\mu_{\text{SY}} = 2.4$ GeV, as done in [2]) and to re-estimate the contribution δ^2 from the next twist term. The influence of both these effects appears to be important and it is examined here in detail. Furthermore, we are not satisfied with the error estimation performed in the SY analysis, for reasons to be explained later, and prefer therefore to use a more traditional treatment to determine the sensitivity to the input parameter δ^2 and the construction of the 1- σ and 2- σ error contours.

Our main goal in the present work will be to obtain new constraints on the (a_2, a_4) DA parameters from the CLEO data, taking into account all the remarks mentioned above, and then to compare them with the constraints following from QCD SRs with nonlocal condensates (NLC). We will not repeat here the derivation of the main results of LCSRs, as well as those related to NLC SRs, but we will refer the interested reader to [3, 2] and correspondingly to [5, 6] and references therein. But for the sake of convenience we included a technical exposition of our approach in comprehensive appendices. The paper is organized as follows. In Sec. 2 we review different QCD approaches to calculate the transition form factor $F^{\gamma^*\gamma\pi}(Q^2)$, having recourse to QCD “factorization theorems” [7], encompassing both perturbation theory and LCSRs. The analysis of the CLEO data is discussed in Sec. 3 in conjunction with the SY approach in comparison with other approaches/approximations. In Sec. 4 we present a complete NLO analysis of the CLEO data with a short discussion of the BLM setting procedure. Sec. 5 includes a comparison of the QCD SR pion DA models with the results obtained in Sec. 4 from the CLEO data processing. In Sec. 6 we summarize our conclusions. The paper ends with five appendices: in Appendix A we re-estimate the value of the twist-four scale δ^2 . In Appendix B the old Chernyak–Zhitnitsky (CZ) result for a_2 is discussed, paying attention to evolution effects. In Appendices C and D the two-loop results [8, 9] for the purely perturbative part of the form-factor calculations and the ERBL evolution of the pion DA are outlined. Finally, in Appendix E, all needed calculation details for the NLO LCSR are presented.

2 Transition form factor $F^{\gamma^*\gamma\pi}(Q^2)$ with LCSR

2.1 Factorization of the $F^{\gamma^*\gamma\pi}$ form factor. Standard results

The form factor of the process $\gamma^*(q_1)\gamma^*(q_2) \rightarrow \pi^0(p)$ is defined by the matrix element

$$\int d^4z e^{-iq_1z} \langle \pi^0(p) | T\{j_\mu(z)j_\nu(0)\} | 0 \rangle = i\epsilon_{\mu\nu\alpha\beta} q_1^\alpha q_2^\beta F^{\gamma^*\gamma\pi}(Q^2, q^2), \quad (1)$$

where $q_1 + q_2 = p$, $Q^2 = -q_1^2 > 0$ with $q^2 = -q_2^2 \geq 0$ are the virtualities of the photons, $j_\mu = (\frac{2}{3}\bar{u}\gamma_\mu u - \frac{1}{3}\bar{d}\gamma_\mu d)$ is the quark electromagnetic current, and $\pi^0(p)$ is the pion state with momentum p . If both virtualities, Q^2 and q^2 , are sufficiently large, the T -product of the currents in (1) can be expanded near the light-cone $z^2 = 0$. This expansion results in factorization theorems, which control the structure of the form factor [7] at leading twist. As a result, the form factor can be cast in the form of a convolution over the momentum fraction variable x (of the total momentum p) to read

$$F_{\text{QCD}}^{\gamma^*\gamma^*\pi}(Q^2, q^2) = f_\pi \int_0^1 dx T(Q^2, q^2; \mu_F^2; x) \varphi_\pi(x; \mu_F^2) \equiv f_\pi T(Q^2, q^2; \mu_F^2; x) \otimes_x \varphi_\pi(x; \mu_F^2). \quad (2)$$

The hard amplitude $T(Q^2, q^2; x)$ – playing the role of the Wilson coefficient in the OPE – is calculable within QCD perturbation theory (PT):

$$T = T_0 + \frac{\alpha_s(\mu_R^2)}{4\pi} T_1 + \left(\frac{\alpha_s(\mu_R^2)}{4\pi} \right)^2 T_2 + \dots, \quad (3)$$

while the pion DA $\varphi_\pi(x; \mu_F^2)$ contains the long-distance effects and demands the application of nonperturbative methods. Due to factorization theorems, DAs enter as the central input of various QCD calculations of hard exclusive processes. The LO term T_0 in (3) depends only on kinematical variables, but the NLO amplitude T_1 , calculated in [8, 9], depends also on the factorization scale μ_F^2 :

$$T_0(Q^2, q^2; x) \equiv N_T C_0(Q^2, q^2; x) = N_T \left[\frac{1}{Q^2 x + q^2(1-x)} + (x \rightarrow 1-x) \right]; \quad (4)$$

$$T_1(Q^2, q^2; \mu_F^2; x) = N_T \left[\ln \left(\frac{\bar{Q}^2}{\mu_F^2} \right) \cdot C_0(Q^2, q^2; u) \otimes_u V_0(u, x) + C_1(Q^2, q^2; x) \right]. \quad (5)$$

Here, $N_T \equiv (e_u^2 - e_d^2)/\sqrt{2} = \sqrt{2}/6$ is the QCD normalization factor, $\bar{Q}^2 = -[(q_1 - q_2)/2]^2 = (Q^2 + q^2)/2$, and μ_R^2 and μ_F^2 denote, respectively, the scale of renormalization of the theory and the factorization scale of the process. $C_{0,1}$ and $V_{0,1}$ are, respectively, the perturbative expansion elements of the coefficient function C of the process and the ERBL kernel V in the LO (subscript 0) and NLO (subscript 1) approximation⁴. The structure of T_1 is discussed in more detail in [9, 10] and in Appendix C.1. Here we only recall those features relevant for our discussion: Eq. (5), which specifies the definition of the coefficient function C_1 is a consequence of the QCD factorization theorems [7]. Due to these theorems, the first logarithmic term in Eq. (5), originating from collinear divergences, can be absorbed into the renormalization of the DA, $\varphi_\pi(x; \mu_F^2)$, following the ERBL equation (see App. D, Eq. (D.1)). Namely, the formal solution of the ERBL equation in the 1-loop approximation is

$$\varphi_\pi(x; \mu_0^2) \xrightarrow{\text{ERBL}} \varphi_\pi^{\text{RG}}(x; \mu^2) = \exp \left[\int_{a_s(\mu_0^2)}^{a_s(\mu^2)} \frac{a da}{\beta(a)} V_0(x, u) \otimes_u \right] \varphi_\pi(u; \mu_0^2) \quad (6)$$

(here $\beta(a) = -b_0 a^2$ is the 1-loop β -function and $a_s(\mu^2) \equiv \alpha_s(\mu^2) b_0/(4\pi)$). Eq. (6) should be understood in the following way

$$\left[V_0(x, u) \otimes_u \right]^n \varphi_\pi(u; \mu_0^2) = V_0(x, u_1) \otimes_{u_1} \dots \otimes_{u_{n-1}} V_0(u_{n-1}, u_n) \otimes_{u_n} \varphi_\pi(u_n; \mu_0^2).$$

⁴wherein V_1 is needed to evolve the pion DA in the NLO approximation.

We adopt here as a factorization scale $\mu_F^2 = Q^2$. For that case, $F^{\gamma^*\gamma^*\pi}$, obtained in Eq. (2) at the scale μ^2 , can be transformed into

$$F^{\gamma^*\gamma^*\pi} \rightarrow F_{\text{RG}}^{\gamma^*\gamma^*\pi}(Q^2, q^2) = f_\pi \left[T_0(Q^2, q^2; x) + \frac{\alpha_s(\mu_R^2)}{4\pi} T_1(Q^2, q^2; Q^2; x) \right] \otimes_x \varphi_\pi^{\text{RG}}(x; Q^2). \quad (7)$$

To fix the renormalization scale μ_R^2 , one needs to go beyond the NLO approximation. In the absence of such information and in order to further simplify the NLO analysis, we also set $\mu_R^2 = \mu_F^2 = Q^2$. It is useful to expand $\varphi_\pi^{\text{RG}}(x; \mu^2)$ over the eigenfunctions $\psi_n(x)$ of the one-loop ERBL equation, i.e., in terms of the Gegenbauer polynomials $C_n^{3/2}(\xi)$,

$$\varphi_\pi^{\text{RG}}(x; \mu^2) = \sum_{n=0,2,4,\dots} a_n(\mu^2) \cdot \psi_n(x); \quad a_0 = 1; \quad \psi_n(x) \equiv 6x(1-x)C_n^{3/2}(2x-1). \quad (8)$$

In this representation, all the dependence on μ^2 is contained in the coefficients $a_n(\mu^2)$ and is dictated by the ERBL equation. Different reasons, explained in [2] and [5, 6], point to the possibility of retaining only the first 3 terms in this expansion. Following then this approximation, the form factor can be parameterized by only two variables $a_2(\mu_0^2)$ and $a_4(\mu_0^2)$ that accumulate the mesonic large-distance effects (at some scale μ_0^2).

A special case of the OPE appears when one of the photons (q_2) is near the mass shell. It is instructive to present here an evident NLO perturbative expression for Eq. (7) in the *formal limit* $q^2 \rightarrow 0$ (cf. Eq. (C.9) in Appendix C),

$$F_{\text{PT}}^{\gamma^*\gamma\pi}(Q^2) = \frac{\sqrt{2}}{Q^2} f_\pi \left[1 + \Sigma(Q^2) + \frac{\alpha_s(Q^2)}{4\pi} C_F (-5 + 7.9 \cdot \Sigma(Q^2) - 3.8 \cdot \Delta(Q^2)) - \frac{80}{27} \frac{\delta^2(Q^2)}{Q^2} \right] \quad (9)$$

with $\Sigma(Q^2) \equiv a_2(Q^2) + a_4(Q^2); \quad \Delta(Q^2) \equiv a_2(Q^2) - a_4(Q^2).$

On the r.h.s. of Eq. (9), the twist-four contribution is included in terms of the twist-four asymptotic DAs, presented in [3]. The coefficients $a_{2,4}(Q^2)$ and the twist-four coupling $\delta^2(Q^2)$ are evolved to the scale Q^2 using, correspondingly, the renormalization group (RG) equation to NLO and LO accuracy⁵.

2.2 Why do we need LCSRs for the transition form factor?

A straightforward calculation of $F^{\gamma^*\gamma\pi}(Q^2)$ in QCD is not possible. In particular, at the formal limit $q^2 \rightarrow 0$, it is not sufficient to retain only a few terms of the light-cone OPE of (1). One has, in addition, to take into account the interaction of the small-virtuality photon at large distances proportional to $O(1/\sqrt{q^2})$, (for a recent discussion, consider section 4 in [4] and [10]). The LCSR method allows one to avoid the problem of the photon long-distance interaction by providing the means of performing all QCD calculations at sufficiently large q^2 and then use a dispersion relation to return to the mass-shell photon. To isolate the dangerous neighborhood of $q^2 = 0$, one should apply an appropriate realistic model for the spectral density at low s , based, for instance, on quark-hadron duality. Using this sort of analysis and by employing analyticity and duality arguments, the following expression was obtained in [3]

$$F_{\text{LCSR}}^{\gamma^*\gamma\pi}(Q^2) = \int_0^{s_0} \frac{ds}{m_\rho^2} \mathbf{Im} \left[\frac{1}{\pi} F_{\text{QCD}}^{\gamma^*\gamma^*\pi}(Q^2, s) \right] e^{(m_\rho^2 - s)/M^2} + \int_{s_0}^{\infty} \frac{ds}{s} \mathbf{Im} \left[\frac{1}{\pi} F_{\text{QCD}}^{\gamma^*\gamma^*\pi}(Q^2, s) \right]. \quad (10)$$

$F_{\text{QCD}}^{\gamma^*\gamma^*\pi}(Q^2, s)$ on the r.h.s. of (10) is taken from Eq. (2) and the Borel parameter is $M^2 \approx 0.7 \text{ GeV}^2$, whereas m_ρ is the ρ -meson mass and $s_0 = 1.5 \text{ GeV}^2$ denotes the effective threshold in the ρ -meson channel.

⁵The reasons for this treatment will be discussed in more detail in Sec. 4.

This program has first been realized in [3] for the leading order approximation of the process. Taking $F_{\text{QCD}}^{\gamma^*\gamma^*\pi}$ at LO in α_s , the form factor $F_{\text{LO LC}}^{\gamma^*\gamma^*\pi}(Q^2)$ was obtained from Eq. (10) with

$$F_{\text{LO QCD}}^{\gamma^*\gamma^*\pi}(Q^2, q^2) = f_\pi N_T \left[C_0(Q^2, q^2; u) \otimes_u \varphi_\pi(u) - \frac{1}{2} [C_0(Q^2, q^2; u)]^2 \otimes_u \varphi_\pi^{(4)}(u) \right] \quad (11)$$

and

$$\mathbf{Im} \left[\frac{1}{\pi} F_{\text{LO QCD}}^{\gamma^*\gamma^*\pi}(Q^2, s) \right] = \frac{f_\pi \sqrt{2}}{3} \left(\frac{\varphi_\pi(u)}{s + Q^2} - \frac{1}{Q^2} \frac{d\varphi^{(4)}(u)}{ds} \right)_{u=Q^2/(s+Q^2)}. \quad (12)$$

Here, the numerically important twist-four contribution was also included using a simple asymptotic expression for the twist-four DA contribution [3]

$$\varphi^{(4)}(u, \mu^2) = \frac{80}{3} \delta^2(\mu^2) u^2 (1-u)^2. \quad (13)$$

Note that the coupling δ^2 is determined from the matrix element

$$\langle \pi(p) | g_s \bar{d} \tilde{G}_{\alpha\mu} \gamma^\alpha u | 0 \rangle = i \delta^2 f_\pi p_\mu. \quad (14)$$

The estimates for $\delta^2(\mu^2)$, including also its RG-evolution, are presented in Appendix A.

2.3 The framework of NLO LCSR for the form factor

A NLO generalization of the above scheme was more recently performed in [2]. The α_s -corrections to this process are expected to be rather large, of the order of 20% (see, e.g., [10]). The size of these corrections can be roughly estimated from the perturbative expressions for their asymptotic parts by comparing to each other the values 1 and $-5 \frac{\alpha_s}{4\pi} C_F$ in Eq. (9). Therefore, for a quantitative description of the form factor, this contribution should be taken into account. This important step was done by Schmedding and Yakovlev, who have used the NLO perturbative expression for $F_{\text{QCD}}^{\gamma^*\gamma^*\pi}$ in Eq. (10),

$$F_{\text{NLO QCD}}^{\gamma^*\gamma^*\pi}(Q^2, q^2; \mu^2) = F_{\text{LO QCD}}^{\gamma^*\gamma^*\pi}(Q^2, q^2) + \frac{\alpha_s(\mu^2)}{4\pi} f_\pi T_1(Q^2, q^2; \mu^2; x) \otimes_x \varphi_\pi(x; \mu^2), \quad (15)$$

where $\mu^2 \equiv \mu_F^2 = \mu_R^2 \neq Q^2$, to construct a NLO version of the LCSR for the form factor $F^{\gamma^*\gamma^*\pi}(Q^2)$. The spectral density $\mathbf{Im}[F_{\text{NLO QCD}}^{\gamma^*\gamma^*\pi}(Q^2, s; \mu^2)]/\pi$, based on Eq. (15), depends on the scale μ^2 . In the original paper [2], this scale was fixed by relating it to the mean value of Q^2 with respect to the CLEO experimental data, i.e., by setting $\mu^2 = \mu_{\text{SY}}^2 = \langle Q_{\text{exp}}^2 \rangle \approx (2.4)^2 \text{ GeV}^2$. Use of Eq. (15) implies that one accounts for the scale dependence in $\varphi_\pi(x; Q^2)$ (e.g., for the different CLEO points) via the leading order perturbative formula

$$\varphi_\pi(x; Q^2) \approx \left[1 + \frac{\alpha_s(\mu^2)}{4\pi} \ln(Q^2/\mu^2) \cdot V_0(x, u) \right] \otimes_u \varphi_\pi(u; \mu^2),$$

rather, than using the RG expression, given by Eq. (6). This seems to be a rather crude approximation, given that other reference points are evolved with μ^2 by utilizing the NLO ERBL evolution equation.

3 CLEO data analysis revisited

Let us scrutinize the form factor approaches, discussed above, in close comparison with the CLEO data [1].

3.1 Theoretical approaches to the CLEO data

In this subsection – in order to be in close analogy with the original SY paper – we shall adopt their scale definition of the CZ DA. It is worth noting, however, that the genuine CZ DA differs from that definition because it is determined at the much lower normalization scale $\mu_0 = 0.5 \text{ GeV}$ (a discussion of this important point is relegated to Appendix B). To distinguish the two models in the present analysis, we will use in what follows a special notation: (i) CZ DA parameters originating from the SY prescription ($a_2^{\text{CZ}}(\mu^2 = 0.5 \text{ GeV}^2) = 2/3$), and by using a 2-loop evolution to the scale μ_{SY}^2 , will be denoted with the superscripts CZSY, whereas (ii) those conforming with our prescription ($a_2^{\text{CZ}}(\mu^2 = 1 \text{ GeV}^2) = 0.56$, see Appendix B) and being 2-loop evolved to the scale μ_{SY}^2 will be marked by the superscripts CZ.

The status of these approximations (NLO PT, LO LCSR and NLO LCSR) is illustrated in Fig. 1 by the relative positions of the corresponding admissible regions for these parameters in the (a_2, a_4) plane. Here, the regions enclosed by the needle-like- and ellipse-like solid contours correspond to a 1σ -deviation criterion (CL=68%) [11], while the broken contours refer to a 2σ -deviation criterion (CL=95%). Note that these contours have been derived by taking into account only the statistical error bars in [1] (see their Table 1). This marks a crucial difference between our processing of the data and that in [2], where the “theoretical-systematic uncertainties” have been involved in the statistical analysis together with the statistical ones. In other words, we do not “smear” the quantities δ^2 (or $a_0 = 1$) over their corresponding (theoretical) error-bar intervals. In our opinion, such a manner would require an additional substantiation and further suggestions about the distribution of these errors that we want to avoid in our analysis. Hence, instead of that, we process the data at a few fixed values of δ^2 in order to clarify the sensitivity of the results to this parameter.

It should be clear that a really admissible region might be somewhat larger than the presented “purely statistical” contours in Fig. 1, a price one has to pay for our strict way of data processing.

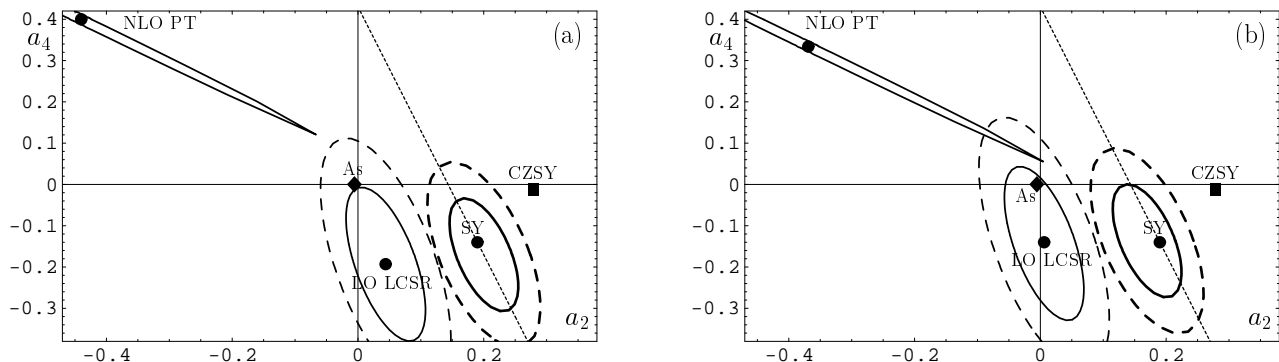


Figure 1: The plane (a_2, a_4) and results of different analyses of the CLEO data for the form factor $F_{\pi\gamma\gamma}(Q^2)$. We show here the best-fit points of LO LCSR, NLO LCSR (SY) and a NLO PT analysis for two values of the twist-four coupling $\delta^2 = 0.2 \text{ GeV}^2$ (a) and $\delta^2 = 0.18 \text{ GeV}^2$ (b). The solid contours correspond to a 1σ -criterion, while the broken ones to a 2σ -criterion. We also plot for comparison the positions of the CZSY (■) and the asymptotic (◆) DAs. All values are evaluated at $\mu^2 = (2.4 \text{ GeV})^2$. The inclined straight line on the right hand-side of the figure is the modified diagonal $a_2 + a_4/3 = \text{CONST}$, corresponding to the new 1σ -ellipse of the NLO LCSR analysis.

- (i) The large contour, enclosing the origin, corresponds to the LO LCSR form factor, discussed in [3]. Note that the point denoting the position of the asymptotic DA lies just on the periphery of the 1σ -contour and that the CZ DA one (see [3]), lies far outside.
- (ii) The needle-like contour on the left top corner of both parts of Fig. 1 corresponds to Eq. (9) and is stretched along the “diagonal” $a_2 + 0.75 \cdot a_4 = \text{CONST}$. The weak dependence of

Eq. (9) on $\Delta \equiv a_2 - a_4$ slightly turns the angle of the diagonal $\simeq 3\pi/4 \rightarrow 0.8\pi$. On the other hand, taking into account the evolution with Q^2 of a_2 and a_4 for every Q_{exp}^2 makes the contour finite – much like a “diagonal” needle-like strip. As we have mentioned above, the formal limit of the NLO expression, Eq. (9), *cannot* give a reliable result for the form factor. In this context it is interesting to mention that the corresponding contour is located outside the regions determined by the LCSRs. Furthermore, all known DA models (see, e.g., Table 3.1) and the phenomenological predictions ([12, 5] and references therein) are located far away from this contour – clearly demonstrating the poor reliability of the corresponding perturbative approach.

- (iii) At least the heavy-line contours (enclosing also the SY point [2]) correspond to the SY approximation. These contours do not overlap with those corresponding to the LO LCSR ones – even at the 2σ -deviation level. Therefore, α_s -corrections are crucially important in extracting the DA parameters. Our best-fit point with respect to the NLO LCSR is close to but not coinciding with the one presented by SY (compare entries 3 and 4 in Table 3.1). In Fig. 1(a) the full circle inside the contour is just the SY point. The best-fit points, corresponding to different approximations and models, considered in the present analysis, are collected in Table 3.1, where the notation $\chi_{(\text{d.o.f.})}^2 = \chi^2/14$ has been used (in correspondence to the number 15 of the CLEO experimental data points).

It should be stressed that the admissible region (heavy-line contours), obtained with our data-processing procedure, differs from that in [2]. Our contours look slightly larger than theirs despite the fact that possible theoretical/systematic uncertainties were not included in our consideration. Just because of this latter reason, our contours possess another orientation relative to those of SY, as one appreciates by comparing Fig. 1(a) and Fig. 2 with Fig. 6 in [2]. Moreover, the CZSY DA model appears to be *seemingly* closer ($\chi^2 = 1.8$) to the best-fit point (0.20, -0.17) than the asymptotic one ($\chi^2 \approx 3$). But the genuine CZ DA with $a_2^{\text{CZ}}(\mu_{\text{SY}}^2) = 0.35$ and $a_4^{\text{CZ}}(\mu_{\text{SY}}^2) = -0.006$ (consult the discussion in Appendix B) generates a value of $\chi^2 = 3.6$, which is larger than that of the asymptotic DA.

Table 3.1: The best-fit points shown in Fig.1(a) with $\delta^2(1 \text{ GeV}^2) = 0.20 \text{ GeV}^2$

Best-fit points/models	$a_2(\mu_{\text{SY}}^2)$	$a_4(\mu_{\text{SY}}^2)$	$\chi_{(\text{d.o.f.})}^2$
NLO PT (9) best fit	-0.44	+0.40	0.49
LO LCSR best fit	+0.04	-0.19	0.48
NLO LCSR best fit	+0.20	-0.17	0.48
SY LCSR [2]	+0.19	-0.14	0.49
BMS model [5]	+0.13	-0.08	0.74
CZSY DA [2]	+0.28	-0.009	1.8
CZ DA [13]	+0.35	-0.006	3.6
Asympt. DA	-0.006	+0.00	3.0

The best-fitted linear combination⁶ of a_2 , a_4 , that determines the large axis of the NLO LCSR contour (see Fig. 1(a)) and parameterizes its orientation, is found to be

$$a_2 + \frac{1}{3} \cdot a_4 = 0.143, \quad (16)$$

⁶Dubbed “diagonal” in what follows.

instead of $a_2 + 0.6 \cdot a_4 = 0.11 \pm 0.03$, reported in [2]. Note that the SY point also belongs to the diagonal: $a_2^{\text{SY}} + 1/3 \cdot a_4^{\text{SY}} \approx 0.143$. The coefficient $1/3$ in (16) can be predicted without any fitting; it is solely determined by the structure of the NLO LCSR (10). Indeed, Eq. (10) can be rewritten as [2]

$$A_0(Q^2, \mu_{\text{SY}}^2) + A_2(Q^2, \mu_{\text{SY}}^2) \cdot a_2(\mu_{\text{SY}}^2) + A_4(Q^2, \mu_{\text{SY}}^2) \cdot a_4(\mu_{\text{SY}}^2) = Q^2 \cdot F^{\gamma^* \gamma \pi}(Q^2),$$

(to be compared with the fit given in Eq. (16)) and the discussed coefficient expresses the average value of the ratio $A_4(Q^2, \mu_{\text{SY}}^2)/A_2(Q^2, \mu_{\text{SY}}^2)$. Notice that this ratio, averaged over the CLEO data range $\{Q_{\text{exp}}^2\}$, amounts to 0.31, while the r.h.s. of Eq. (16) is determined by the experimental data on the form factor. The coefficient 0.6, obtained in the SY fit [2], can be associated with the same ratio at the mean value $\mu_{\text{SY}}^2 = \langle Q_{\text{exp}}^2 \rangle$. The ratio $A_4(Q^2)/A_2(Q^2)$ is a concave function in Q^2 and, therefore, its mean value, $\langle A_4(Q^2)/A_2(Q^2) \rangle$, is smaller than its value, $A_4(\mu_{\text{SY}}^2)/A_2(\mu_{\text{SY}}^2)$, at the “mean point” μ_{SY}^2 .

3.2 Sensitivity to input parameters

As it turns out, the location of the admissible a_2 , a_4 regions is rather sensitive to the value of the input parameter δ^2 . To illustrate this point, we have repeated the data processing with an admissible (near its low boundary) value $\delta^2 = 0.18 \text{ GeV}^2$ (see Appendix A). All contours in Fig. 1(b) shift closer to the asymptotic point (\blacklozenge), but their relative positions do not drastically change and, hence, the main conclusions (i-iii) of the previous subsection remain valid. The results of this data processing are presented in Fig. 1(b) and in Table 3.2. One appreciates that the hierarchy of the different models (lower parts of both Tables) with respect to the NLO LCSR best fit does not change, though the values of χ^2 can change significantly. Indeed, the point marking the BMS model moves from the 2σ -deviation level at $\delta^2 = 0.2 \text{ GeV}^2$ (see Table 3.1) inside the 1σ -deviation region near the SY LCSR point at $\delta^2 = 0.18 \text{ GeV}^2$ (cf. row 5 in Table 3.2). Therefore, the value of δ^2 and, in general, also the value of the twist-four term can substantially affect the locations of the admissible regions. But all other options, like the CZ DA and the asymptotic DA, remain excluded at the 2σ -deviation level.

Table 3.2: The best fit points shown in Fig. 1(b) with $\delta^2(1 \text{ GeV}^2) = 0.18 \text{ GeV}^2$

Best-fit points/models	$a_2(\mu_{\text{SY}}^2)$	$a_4(\mu_{\text{SY}}^2)$	$\chi_{(\text{d.o.f.})}^2$
NLO PT (9) best fit	-0.37	+0.34	0.49
LO LCSR best fit	+0.006	-0.14	0.49
NLO LCSR best fit	+0.17	-0.14	0.48
SY LCSR [2]	+0.19	-0.14	0.51
BMS model [5]	+0.13	-0.08	0.56
CZSY DA [2]	0.28	-0.009	2.2
CZ DA [13]	+0.35	-0.006	4.2
Asympt. DA	-0.006	+0.00	2.3

Let us pause for a moment and turn our attention to a recent paper by Diehl et al. [14]. The authors of this work employ a purely perturbative QCD approach to analyze the CLEO data without taking into account the twist-four contribution, i.e., using Eq. (9) with $\delta^2(Q^2) = 0$. Comparing their results with those of Schmedding and Yakovlev [2], Diehl et al. correctly note that the relative weights of $a_2(\mu_0^2)$ and $a_4(\mu_0^2)$ in $F^{\gamma^* \gamma \pi}$ display a much stronger Q^2 -dependence than in the leading-twist case with the consequence that the allowed SY parameter region becomes much

smaller than in their approach. However, there seems to be a confusion concerning the inclusion of uncertainties in the Schmedding–Yakovlev analysis. While Diehl et al. claim that no error was assigned to the input of twist-four DA, Schmedding and Yakovlev do indeed allow for an uncertainty of $\pm 20\%$ for the twist-four contribution. In our analysis we use a different approach: the value of δ^2 is connected with the parameter λ_q^2 of the vacuum non-locality. We first fix the value of λ_q^2 and then we allow for the parameter δ^2 to vary in a 10% range. The whole uncertainty in δ^2 for the selected range of $\lambda_q^2 = 0.4 - 0.6 \text{ GeV}^2$ amounts then to about 30% in accordance with [15]. This strategy enables us to use the CLEO data as a direct measure (a vacuum detector) to select that model for the QCD vacuum, which provides the best agreement between theory and experiment.

4 Complete two-loop analysis of the CLEO data

In the previous section we have demonstrated the high sensitivity of the DA parameters (a_2 , a_4) to strong radiative corrections for the form factor, as well as to the scale of the twist-four contribution (see Fig. 1 a(b) and [5]). Therefore, to obtain these parameters from the CLEO data in a reliable way, one should take into account the radiative corrections in the most accurate possible way. To this end, we want to improve in this section the accuracy of the extraction procedure of (a_2 , a_4) at the NLO level. A new estimate for δ^2 , the magnitude of the twist-four contribution, is also introduced in the present analysis (see below). We also briefly discuss an attempt *to go beyond* the level of the NLO, having recourse to a recent calculation [16] of the radiative correction based on the BLM scale setting.

4.1 Complete NLO analysis

Here we use the complete 2-loop expression for the form factor $F^{\gamma^*\gamma^*\pi}(Q^2, q^2)$, given by Eq. (7). For this reason, we put $\mu^2 = Q^2$ in (15) so that for the quantities

$$\alpha_s(\mu^2) \xrightarrow{\text{RG}} \alpha_s(Q^2), \quad \varphi_\pi(x; \mu^2) \xrightarrow{\text{ERBL}} \varphi_\pi(x; Q^2) = U(\mu^2 \rightarrow Q^2) \varphi_\pi(x; \mu^2),$$

the NLO evolution is implied. Then, we substitute the spectral density $\rho(Q^2, s; \mu^2 = Q^2)$, derived in [2] (see the text below Eq. (15)), in LCSR (10) to obtain $F^{\gamma^*\gamma\pi}(Q^2)$ in a regular manner and to fit the CLEO data over $Q^2 \in \{Q_{\text{exp}}^2\}$. The evolution $\varphi_\pi(x; Q^2) = U(\mu_{\text{SY}}^2 \rightarrow Q^2) \varphi_\pi(x; \mu_{\text{SY}}^2)$ is performed *for every point* Q_{exp}^2 , with the aim to return to the normalization scale μ_{SY}^2 and to extract the DA parameters (a_2 , a_4) at this reference scale. Stated differently, for every measurement, $\{Q_{\text{exp}}^2, F^{\gamma^*\gamma\pi}(Q_{\text{exp}}^2)\}$, its own factorization/renormalization scheme has been used so that the NLO radiative corrections are taken into account in a complete way.

The accuracy of the procedure is, nevertheless, still limited owing to the mixing of the NLO and the LO approximations. Indeed, the value of the twist-four coupling $\delta^2(\mu^2)$, as well as its RG-evolution with μ^2 , are estimated in the LO approximation. This quantity enters the LCSR formula (15) together with the NLO-part and can lead to an additional uncertainty. In order to improve the theoretical accuracy of the values of a_2 and a_4 , extracted from the CLEO data, one has to re-estimate the twist-four contribution, $\delta^2(1 \text{ GeV}^2)$, with a better accuracy.

To summarize, our data processing procedure differs from the SY one in the following points:

1. $\alpha_s(\mu^2)$ is the exact solution of the 2-loop RG equation, rather than the approximate (but popular in the HEP community) expression (C.16) [11], that was used in the SY analysis.
2. All logarithms $\ln(Q^2/\mu^2)$ are absorbed into the evolution of the pion DA, performed separately at each experimental point Q_{exp} (compare Eqs. (6), (7) with Eq. (15)). The corresponding expressions for the form factor are collected in Appendix E.

3. The value of the parameter δ^2 has been re-estimated to read $\delta^2(1\text{GeV}^2) = 0.19 \pm 0.02 \text{ GeV}^2$ (see Appendix A), and this value has been used in the data processing.

This processing of the CLEO data produces the admissible regions, one of which, corresponding to $\delta^2 = 0.19 \text{ GeV}^2$, is shown in Fig. 2(a), where the original SY regions (Fig. 6 in [2]) are also presented in Fig. 2(d) for the ease of comparison. To produce the complete 2σ - and 1σ -contours, corresponding to $\delta^2(1\text{GeV}^2) = 0.19 \pm 0.02 \text{ GeV}^2$, we need to unite three regions obtained for different values of the twist-four parameter: $\delta^2 = 0.17, 0.19, 0.21 \text{ GeV}^2$. This procedure is illustrated in Fig. 2(b) using as an example the 2σ -contour. Let us remind the reader in this context that the SY contours are stretched along the ‘‘LO perturbative’’ diagonal $a_2 + a_4 = \text{CONST}$ (the dashed straight line on the l.h.s. resembles exactly this diagonal) while the solid (dotted) contours correspond to the 1σ (2σ) regions. This stretching of the contours appears here because of the SY manner of the data processing, namely, because the theoretical uncertainties of the input parameters were also involved in the statistical analysis.

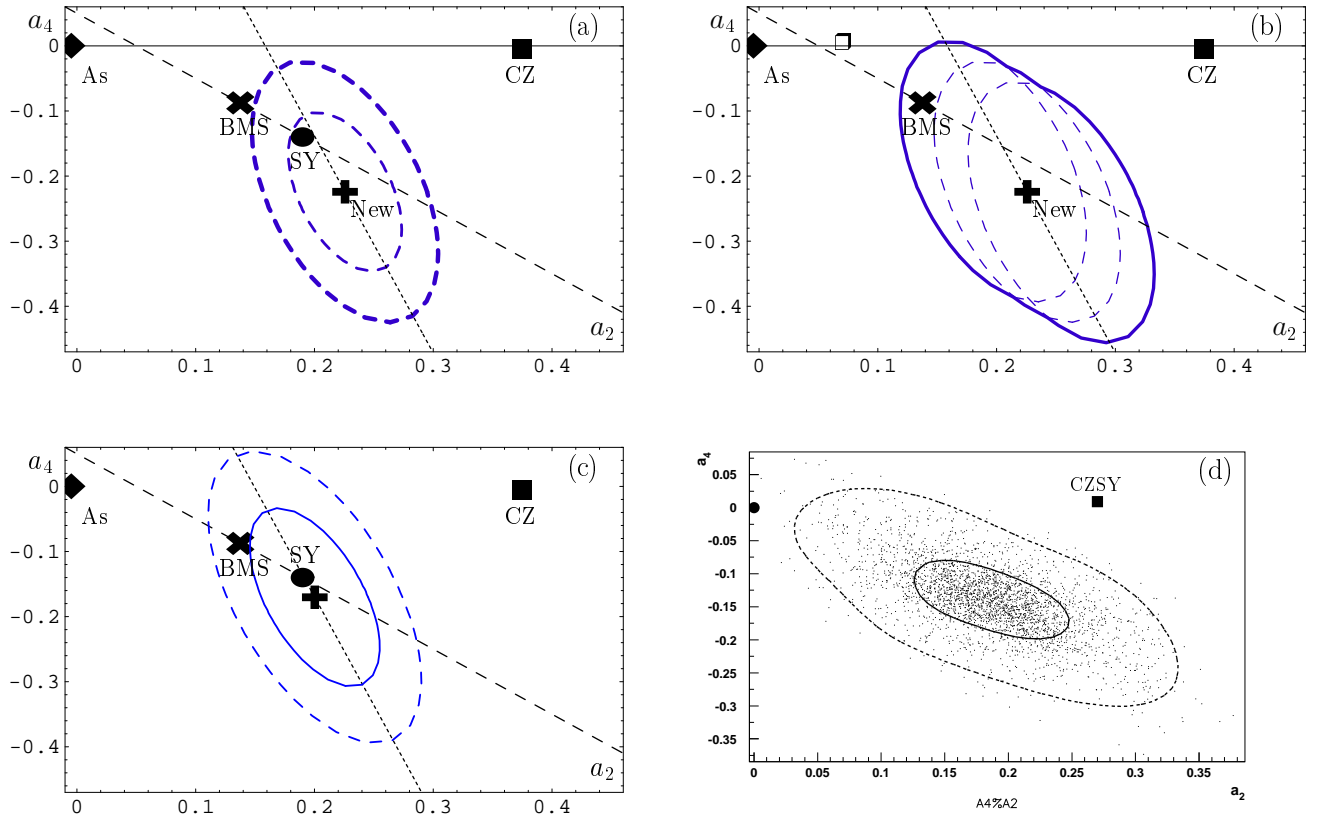


Figure 2: Results of the analysis of the CLEO data for the form factor $F_{\pi\gamma^*\gamma}(Q^2)$ in terms of fiducial areas in the plane (a_2, a_4) . (a) We show the best fit point of the new NLO LC SRs (⊕, termed ‘‘New’’, which is associated with the value of the twist-four coupling $\delta^2 = 0.19 \text{ GeV}^2$, and display by the heavy (broken) contour the regions corresponding to a 1σ (2σ)-deviation. We also show the SY point (●), the BMS point (⊗), the asymptotic point (◆), and the CZ point (■) - all evolved to the SY scale. The inclined straight dotted line in the left figure is the modified diagonal $a_2 + 0.3a_4 = 0.159$, whereas the inclined straight dashed line is the original diagonal $a_2 + a_4 = \text{CONST}$. (b) We show three 2σ -regions (dashed contours), obtained for different values of the twist-four parameter: $\delta^2 = 0.17, 0.19, 0.21 \text{ GeV}^2$ and also their unification: 2σ -contour (thick line). All points and straight lines are as in Fig. 2(a), except □, which denotes a brand-new result obtained on a transverse lattice [17]. (c) The contours of the previous NLO analysis *à la* SY and the ‘‘old’’ best-fit point (⊕) are presented for comparison (cf. the lower right corner of Fig. 1(a) and use the scale of Fig. 2(a)). (d) The original SY plot (note the different scales on the axes and the symbol ■ denoting the CZSY DA) is shown for comparison. All values shown are evaluated at the scale $\mu = 2.4 \text{ GeV}$.

The new best-fit point (⊕, ‘‘New’’), as well as the whole σ -contours themselves appear to be

displaced in Fig. 2(a) (approximately) along the new diagonal (cf. Eq. (16)),

$$a_2 + 0.3 \cdot a_4 = 0.16 \pm 0.007. \quad (17)$$

In Fig. 2(c) we present for comparison the contours of the previous NLO analysis in the sense of SY (low right corner of Fig. 1(a)) drawn, however, at the scale of Fig. 2(a). The positions of the best-fit points and models are provided in Table 4.1. It should be clear from our discussion that these new contours are somewhat smaller than the previous ones (Fig. 2(c)), but slightly larger than the original SY ones (Fig. 2(d)), and show another orientation along the diagonal Eq. (17). The difference between the new regions, determined in the present analysis, and those of the SY one is remarkable. For instance, the SY point appears now near the boundary and inside the 1σ -region in Fig. 2(a). Moreover, the preliminary (i.e., for $a_4 = 0$) SY best-fit point, $a_2' = 0.12 \pm 0.03$ [2], and the phenomenological estimates for (a_2, a_4) , presented in [12], ($a_4 = 0$, $a_2 (1 \text{ GeV}^2) = 0.1 \pm 0.1$), lie on the boundary of the united 2σ -region (see Fig. 2(b)).

Table 4.1: Best-fit points shown in Fig. 2(a) with $\delta^2(1 \text{ GeV}^2) = 0.19 \text{ GeV}^2$

Best-fit point/models	$a_2(\mu_{\text{SY}}^2)$	$a_4(\mu_{\text{SY}}^2)$	$\chi_{(\text{d.o.f.})}^2$	$a_2 + 0.3 \cdot a_4$
New NLO LCSR best fit	+0.23	-0.22	0.47	0.159
SY NLO LCSR [2]	+0.19	-0.14	0.59	0.153
BMS model [5]	+0.14	-0.09	1.0	0.113
Asymptotic model	-0.002	+0.00	4.3	-0.00
CZ model [13]	+0.43	-0.003	4.3	0.43

4.2 Beyond the NLO approximation: effects from BLM scale-setting

The renormalization scale μ_R^2 in Eq. (7) can be fixed by a NNLO calculation of T_2 following the BLM prescription. Recently, the NNLO contribution to C_2 , proportional to b_0 and required for the BLM scale setting, was obtained in [16] for a kinematics with $q_2^2 = 0$. As an exercise, let us perform the new fit to obtain the scale $\mu_R^2 = \mu_{\text{BLM}}^2$ and the best-fit point $\{a_2^{\text{BLM}}, a_4^{\text{BLM}}\}$ for the NLO expression given by Eq. (9). We follow the same procedure as in Sec. 3.1, replacing this time $\alpha_s(Q^2) \rightarrow \alpha_s(\mu_{\text{BLM}}^2(a_2, a_4, Q^2))$ in Eq. (9), where for $\mu_{\text{BLM}}^2(a_2, a_4, Q^2)$ Eq. (7.7) from [16] is used. As it turns out, practically for all points in the considered domain in the lower half-plane $a_4 \leq 0$, the BLM setting leads to the condition $\mu_{\text{BLM}}^2 \ll Q^2$, in conformance with the results of [16]. Therefore, for this region, the BLM setting seems to rule out predictions from the NLO perturbation theory.

Only for points within a rather thin strip in the upper half-plane $a_4 > 0$ (cf. Eqs. (7.2a), (7.7) in [16]), the BLM setting gives $\mu_{\text{BLM}}^2 > Q^2$. Interestingly, the case discussed in Sec. 3.1 (ii) and based on Eq. (9) belongs just to this thin strip. The corresponding (a_2, a_4) values are displayed below for comparison together with the initial result (second row) without the BLM setting.

$$\begin{aligned} a_2^{\text{BLM}}(\mu_{\text{SY}}^2) &= -0.55, & a_4^{\text{BLM}}(\mu_{\text{SY}}^2) &= 0.48 & \mu_R^2 &= \mu_{\text{BLM}}^2 \approx Q^2/0.35 \\ a_2(\mu_{\text{SY}}^2) &= -0.44, & a_4(\mu_{\text{SY}}^2) &= 0.40 & \mu_R^2 &= Q^2. \end{aligned} \quad (18)$$

To calculate the imaginary part $\text{Im}F_{\text{QCD}}^{\gamma^*\gamma^*\pi}(Q^2, s)$, used in Eq. (10), one needs to know the NNLO contribution proportional to b_0 for $q_2^2 \neq 0$, which is still not computed. For this reason, the results obtained with the BLM scale setting fall out of the region of the NLO LCSR analysis. The calculation of the complete NNLO contribution or, at least, its convolution with φ_{as} is a very demanding task that has not been accomplished yet.

5 Pion DA from QCD SR vs CLEO data

Let us now turn to the important topic of whether the CLEO data is consistent with the non-local QCD SR results for φ_π . We present in Fig. 3 the results of the data analysis for three central values of the coupling $\delta^2(\mu^2 = 1 \text{ GeV}^2) = 0.19, 0.235, 0.29 \text{ GeV}^2$, which in turn correspond to three admissible values of the vacuum non-locality parameter $\lambda_q^2 = 0.4, 0.5, 0.6 \text{ GeV}^2$. For each value of λ_q^2 from this ensemble, we define the corresponding central value of δ^2 and its uncertainty (for details, see Appendix A). Then, we process the CLEO data as described in the previous section and obtain the complete 2σ - and 1σ -contours on the plane (a_2, a_4) , following from the CLEO experiment. An example of these regions is represented in Fig. 2(b) and is also displayed in Fig. 3(a), where the 2σ -contour is shown as a solid line and the 1σ -contour as a dashed one.

The task now is to compare these new constraints with those following from the QCD SRs with nonlocal condensates. We have established in [5] that a two-parameter model $\varphi_\pi(x; a_2, a_4)$ really enables one to fit all the moment constraints for $\langle \xi^N \rangle_\pi$ that result from NLC QCD SRs (see [18] for more details). The only parameter entering the NLC SRs is the correlation scale λ_q^2 in the QCD vacuum, known from nonperturbative calculations and lattice simulations (for a discussion and references, see Appendix A).

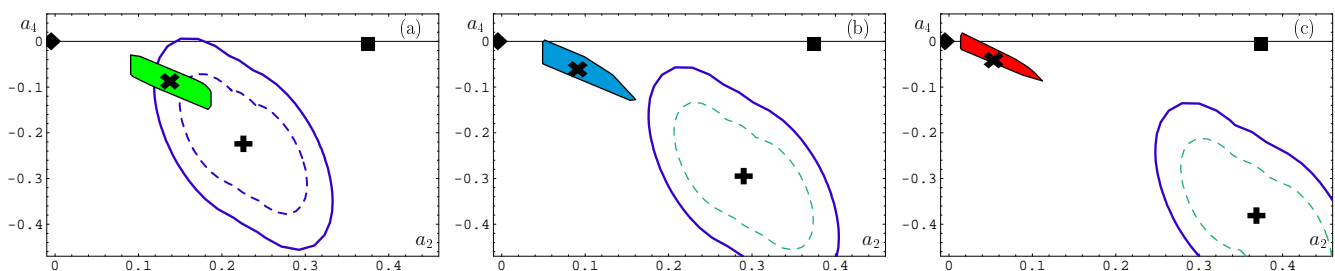


Figure 3: Three 2σ -contours of the admissible regions following from the analysis of the CLEO data for different values of δ^2 : (a) – for $\lambda_q^2 = 0.4 \text{ GeV}^2$ and $\delta^2 = (0.19 \pm 0.02) \text{ GeV}^2$; (b) – for $\lambda_q^2 = 0.5 \text{ GeV}^2$ and $\delta^2 = (0.235 \pm 0.025) \text{ GeV}^2$; (c) – for $\lambda_q^2 = 0.6 \text{ GeV}^2$ and $\delta^2 = (0.29 \pm 0.03) \text{ GeV}^2$. Solid lines in all figures enclose the 2σ -contours, whereas the 1σ -contours are enclosed by dashed lines. The three slanted and shaded rectangles represent the constraints on (a_2, a_4) posed by the QCD SRs [5] for corresponding values of $\lambda_q^2 = 0.4, 0.5, 0.6 \text{ GeV}^2$ (from left to right). All values are evaluated at $\mu = 2.4 \text{ GeV}$ after evolution. The marked points are explained in Fig. 2, except for the point marked with \mathbf{X} . This point represents here the BMS solution, which corresponds to a particular value of λ_q^2 .

The three slanted and shaded rectangles in Fig. 3 are the constraints on the Gegenbauer coefficients (a_2, a_4) resulting from the NLC QCD SRs at different values of $\lambda_q^2 = 0.4, 0.5, 0.6 \text{ GeV}^2$, [5, 6]. The overlap of the displayed regions in Fig. 3 can serve as a means of determining the appropriate value of λ_q^2 . In fact, one may conclude that the value $\lambda_q^2 = 0.4 \text{ GeV}^2$ is more preferable relative to the higher values of λ_q^2 . It should be noted, however, that even for this lowest value of that scale, the agreement with the constraints in Fig. 3 is rather moderate and of similar quality as using the SY constraints [5, 6]. It is tempting to test even smaller values of λ_q^2 than 0.4 GeV^2 in the NLC SR as an attempt to improve the agreement with the CLEO constraints in Fig. 3. But such values appear to be at the lower limits for the λ_q^2 estimates from non-perturbative approaches (see Appendix A). Furthermore, the NLC SR becomes unstable at such low values of λ_q^2 . As a result, the accuracy of the DA moments is rather poor and the final constraint on (a_2, a_4) becomes unreliable. Taking into account all these arguments, we think that an improvement of the ingredients of the NLC ansatz may provide a better agreement with the CLEO data than just using $\lambda_q^2 < 0.4 \text{ GeV}^2$.

6 Conclusions

In this paper we have studied the theoretical predictions for the pion transition form factor $F^{\gamma^*\gamma\pi}(Q^2)$ in comparison with the CLEO experimental data [1] on this form factor. We have presented a full analysis of this data and contrasted the results with those found in the context of QCD LCSR at the NLO level. In this way, we have revised and improved the procedure of analyzing the CLEO data, first performed by Schmedding and Yakovlev in [2]. The main goal has been to obtain constraints on the shape of the pion DA of twist-2, $\varphi_\pi(x; a_2, a_4)$ in the most accurate way. The values of the crucial parameters, viz. the twist-four coupling $\delta^2(\mu^2)$ and $\alpha_s(\mu^2)$, involved in this procedure, have been treated more accurately than in previous approaches. The main findings may be summarized as follows.

1. We have tested different kinds of approximations to calculate $F^{\gamma^*\gamma\pi}(Q^2)$ and revealed how the size of α_s and the twist-four corrections can affect the admissible regions of the DA parameters (a_2, a_4) .
2. New admissible regions for the (a_2, a_4) parameters, see Figs. 2(b), 3(a), – different from those in [2] – have been obtained, though the constraints do not change drastically in the sense that the initial SY best-fit point still belongs to a 1σ -deviation region (CL=68%) in this space, whereas the CZ DA and also the asymptotic one are definitely excluded at the level of a 2σ -deviation criterion (CL=95%). Moreover, one may appreciate by comparing Figs. 2(a, b) with Fig. 2(d) that this exclusion with respect to the asymptotic DA becomes even more pronounced using our data processing.
3. The bunch of admissible pion DAs, $\varphi_\pi^{BMS}(x; a_2, a_4)$, corresponding to the estimate $\lambda_q^2 = 0.4$ GeV², that was constructed within the framework of QCD SRs with nonlocal condensates in [5], compares well (at the 2σ -level) with the new more restrictive constraints obtained in the present investigation as Fig. 3 demonstrates. In addition, half of the calculated admissible region intersects with the 1σ domain as well, see Fig. 3(a).

Acknowledgments. This work was supported in part by the Russian Foundation for Fundamental Research (contract 00-02-16696), INTAS-CALL 2000 N 587, the Heisenberg–Landau Programme (grants 2002-15 and 2001-11), and the COSY Forschungsprojekt Jülich/Bochum. We are grateful to A. Kotikov, A. Nagaitsev, K. Passek, A. Radyushkin, D. V. Shirkov, A. Sidorov, M. Strikman, and O. Teryaev for discussions and O. Yakovlev for correspondence. One of us (A. B.) is indebted to Prof. Klaus Goeke for the warm hospitality at Bochum University, where this work was partially carried out.

Appendix

A Revision of the QCD SR results for δ^2

The coupling $\delta^2(\mu^2)$ was originally estimated in [19] and found to be $\delta^2(\mu^2 = 1 \text{ GeV}^2) = 0.2 \pm 0.02 \text{ GeV}^2$. Here, we re-analyze the QCD SR for δ^2 , derived in [20], which is based on a non-diagonal correlator of the quark-gluon and quark (pseudoscalar) currents. This SR relates δ^2 to λ_q^2 and determines the value of the ratio $r = \frac{\lambda_q^2}{2\delta^2}$. Evaluating the SR leads to the estimate $r > 1$ and consequently to $\lambda_q^2/2 > \delta^2$. Moreover, r is rather sensitive to the size of the radiative corrections. In this work, we use $\Lambda_3^{\text{LO}} = 312 \text{ MeV}$, obtained recently in a DIS fit of the CCFR data in [21] that leads to $\alpha_s^{\text{LO}}(1 \text{ GeV}^2) \approx 0.59$. The same sort of analysis in the NLO approximation leads to the estimate $\Lambda_3^{\text{NLO}} = 410 \text{ MeV}$ ⁷ that is indeed not far from the standard value 380 MeV (Appendix C.2).

To determine δ^2 , we first fix the parameter λ_q^2 by employing the ‘‘conservative estimate’’ $\lambda_q^2(\mu^2 = 1 \text{ GeV}^2) = 0.4 \text{ GeV}^2$. In QCD the value of this parameter was estimated in the QCD SR approach [22] and also using lattice data [6]:

$$\lambda_q^2 = \frac{\langle \bar{q}(0) \nabla^2 q(0) \rangle}{\langle \bar{q}(0) q(0) \rangle} \underset{\text{limit}}{\overset{\text{in chiral}}{=}} \frac{\langle \bar{q}(0) (ig \sigma_{\mu\nu} G^{\mu\nu}) q(0) \rangle}{2\langle \bar{q}(0) q(0) \rangle} = \begin{cases} 0.4 \pm 0.1 \text{ GeV}^2 & [22, 20] \\ 0.4 - 0.5 \text{ GeV}^2 & [6] \end{cases} . \quad (\text{A.1})$$

A brief review of the different estimates of λ_q^2 is given in [6].

The evaluation of the SR for the quantity r ,

$$\frac{\lambda_q^2}{2\delta^2} \equiv r(M^2, \varrho, s_0) = \frac{1 - \varrho \cdot \exp[-m_{\pi'}^2/M^2]}{1 + \frac{2\pi^2}{9} \frac{\langle G^2 \rangle}{\lambda_q^2 M^2} - \frac{2\alpha_s(1 \text{ GeV}^2)}{3\pi} \frac{M^2}{\lambda_q^2} (1 - \exp[-s_0/M^2])} \quad (\text{A.2})$$

for the standard value of the gluon condensate $\langle G^2 \rangle \equiv \langle \alpha_s GG \rangle / \pi = 0.012 \text{ GeV}^4$, [23], and with

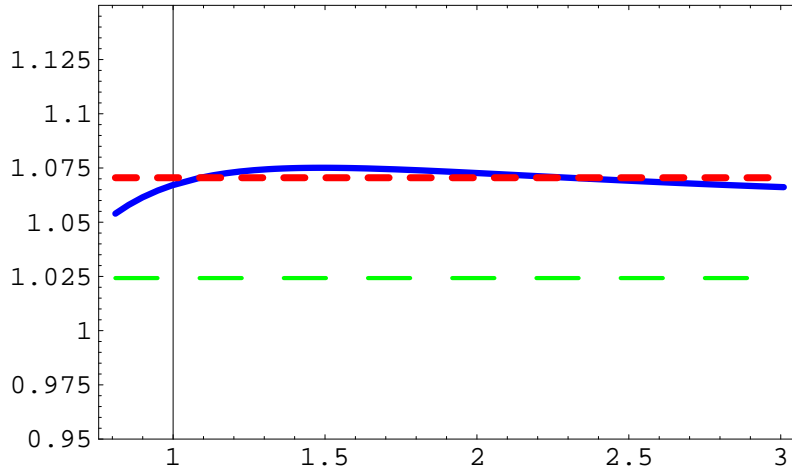


Figure 4: The solid line denotes $r(M^2, \varrho, s)$ for the best-fitted parameters $\varrho = 1.1$, $s_0 = 3.24$. The short-dashed line corresponds to the value $r = 1.07$, whereas the long-dashed line corresponds to r calculated with $\Lambda_3 = 200 \text{ MeV}$.

the fitting parameters, i.e., the coupling to the π' , $\varrho \approx 1.1$, and the duality interval $s_0 = 3.24 \text{ GeV}^2$ yields

$$r = 1.07(\pm 0.01) \Rightarrow \delta^2 \approx 0.19 \text{ GeV}^2 \text{ for } \Lambda_3^{\text{LO}} = 0.312 \text{ MeV} . \quad (\text{A.3})$$

⁷Using the values $\Lambda_4^{\text{LO}} = 265 \text{ MeV}$ and $\Lambda_4^{\text{NLO}} = 340 \text{ MeV}$ given in [21] for $N_f = 4$, we re-calculated the values for $N_f = 3$, i.e., $\Lambda_3^{\text{LO}} = 312 \text{ MeV}$ and $\Lambda_3^{\text{NLO}} = 410 \text{ MeV}$.

The stability of the SR (A.2) with respect to the Borel parameter M^2 is rather good, as the solid line in Fig. 4 clearly effects.

Note that adopting the popular option $\Lambda_3^{\text{LOpop}} = 200$ MeV, it simply imitates the $\alpha_s^{\text{NLO}}(\mu^2)$ behavior at intermediate scales μ^2 , providing $r = 1.02(\pm 0.01)$ and $\delta^2 \approx 0.20$ GeV². This old estimate [20] is also presented here for comparison (cf. long-dashed line in Fig. 4). The parameter r is also rather sensitive to the value of $\langle G^2 \rangle$. For example, the new estimate of the mean value $\langle G^2 \rangle = 0.009$ GeV⁴, suggested quite recently in [24], leads to $r \simeq 1.1$ and $\delta^2 \simeq 0.18$ GeV². Taking into account the last estimate, we derive the uncertainty $\Delta_G \delta^2 \simeq 0.01$ GeV². The other uncertainties, inherent in the SR method (A.2), result to an overall effect of the same order: viz., $\Delta \delta^2 \simeq 0.01$ GeV². Finally, we can establish for δ^2 an accuracy: $\delta^2 = (0.19 \pm 0.02)$ GeV² for $\lambda_q^2 = 0.4$ GeV².

In the same way we obtain from (A.1) the corresponding central values and uncertainties of δ^2 for the higher value of $\lambda_q^2 = 0.5$ GeV² ($\delta^2 = 0.235 \pm 0.025$) and analogously for the value $\lambda_q^2 = 0.6$ GeV² ($\delta^2 = 0.29 \pm 0.03$ GeV²), the latter being of interest due to instanton models [25, 26].

The one-loop anomalous dimension of δ^2 is $\gamma_{T4} = 32/9$ (see, for instance, [12]). On the other hand, the one-loop scale dependence of $\delta^2(\mu^2)$ is given by

$$\delta^2(\mu^2) = \left(\frac{\alpha_s(\mu^2)}{\alpha_s(\mu_0^2)} \right)^{\gamma_{T4}/b_0} \delta^2(\mu_0^2). \quad (\text{A.4})$$

B CZ DA normalization point

The authors of [2] used as a normalization point for the CZ DA the scale $\mu_1^2 = 0.5$ GeV², which is significantly larger than the original one used by Chernyak and Zhitnitsky: $\mu_{\text{CZ}}^2 = 0.25$ GeV². This latter and rather low normalization point is due to the fact that CZ employed the description of charmonium decays, where the characteristic virtuality of the pion is indeed of this low order as μ_{CZ}^2 . Furthermore, in order to construct their model at such a low scale, they evolved the 2nd moments, determined at a scale of 1.5 GeV², down to this scale using 1-loop evolution equations with $\Lambda_{\text{QCD}} = 100$ MeV. The result is the well-known CZ DA:

$$\varphi_{\text{CZ}}(x; \mu_{\text{CZ}}^2) = 6x(1-x) \left[1 + \frac{2}{3} C_2^{3/2} (2x-1) \right] = 30x(1-x)(1-2x)^2. \quad (\text{B.1})$$

However, if one wants to know the shape of this model at another scale, one has to evolve it to that scale. But a natural question arises: what evolution equation should be used to do that?

From our point of view, the best solution would be to determine once and for all the value of the second Gegenbauer coefficient of the CZ DA at the standard QCD SR scale, $\mu_0^2 = 1$ GeV², which is, also according to the CZ arguments, rather close to the scale of the second moment, 1.5 GeV². In this sort of determination, one needs to evolve from the CZ scale μ_{CZ}^2 to the scale $M^2 = 1.5$ GeV² of the second moment $\langle \xi^2 \rangle_{\text{CZ}}$ using the same 1-loop evolution equations (with $\Lambda_{\text{QCD}} = 100$ MeV) as in their original paper [27]. This produces

$$a_2^{\text{CZ}}(\mu^2 = 1.5 \text{ GeV}^2) = 0.51. \quad (\text{B.2})$$

But after restoring this way the CZ model at a scale of 1.5 GeV², we should use for the evolution to 1 GeV² the actual value of the 1-loop QCD scale, i.e., 312 MeV. This gives

$$a_2^{\text{CZ}}(\mu^2 = 1 \text{ GeV}^2) = 0.56. \quad (\text{B.3})$$

C Radiative corrections

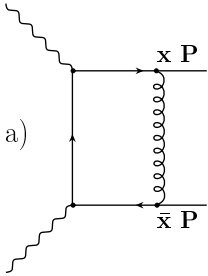
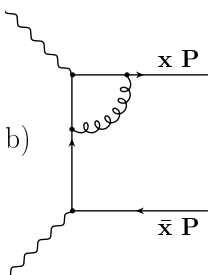
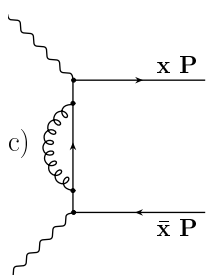
C.1 Structure of the NLO amplitude $T_1(Q^2, q^2; \mu^2; x)$

Here we present diagram bper diagram the results of the NLO T_1 calculation, performed in [9] in the Feynman gauge using the “naive- γ_5 scheme” [8, 16]. To make the presentation more compact, the average virtuality \bar{Q}^2 and the asymmetry parameter ω

$$\bar{Q}^2 = \frac{Q^2 + q^2}{2}, \quad \omega = \frac{Q^2 - q^2}{Q^2 + q^2}, \quad (\text{C.1})$$

have been used, employing also the notation $\bar{x} \equiv 1 - x$.

Table C.1: NLO results for individual diagrams⁸

Diagram	$T_1 = N_T [\log\text{-part} + C_1]$	
	$\ln [\bar{Q}^2/\mu^2]\text{-part}$	$C_1(x, \omega)$
 <p>a)</p> <p>⊕ CROSS</p>	$\ln \left[\frac{\bar{Q}^2}{\mu_F^2} \right] C_0(u, \omega) \otimes_u V_a(u, x)_+ + \ln \left[\frac{\bar{Q}^2}{\mu_F^2} \right] C_0(x, \omega)$	$C'_0(u, \omega) \otimes_u V_a(u, x)_+ + C'_0(x, \omega)$
 <p>b)</p> <p>⊕ M.C. ⊕ CROSS</p>	$\ln \left[\frac{\bar{Q}^2}{\mu_F^2} \right] C_0(u, \omega) \otimes_u V_b(u, x)_+ - 2 \ln \left[\frac{\bar{Q}^2}{\mu_R^2} \right] C_0(x, \omega)$	$\left[C'_0(u, \omega) - C_0(u, \omega) \right] \otimes_u V_b(u, x)_+ - 2C_0(x, \omega) + \left[\ln(1 + \omega[\bar{u} - u]) \otimes_u \left(\frac{V_b(u, x)_+ + K(u, x)}{\bar{Q}^2(1 + \omega[\bar{x} - x])} \right) + (x \rightarrow \bar{x}) \right]$
 <p>c)</p> <p>⊕ CROSS</p>	$\ln \left[\frac{\bar{Q}^2}{\mu_R^2} \right] C_0(x, \omega)$	$C'_0(x, \omega) - C_0(x, \omega)$

⁸M.C. near a diagram denotes the mirror conjugated diagram, cross - the diagram with crossed quark legs.

The results are expressed in terms of the LO coefficient function $C_0(x, \omega)$ (see Eq. (4)) and its logarithmic modification $C'_0(x, \omega)$, naturally appearing in NLO calculations,

$$C_0(x, \omega) = \frac{1}{Q^2} \frac{1}{1 + \omega[\bar{x} - x]} + (x \rightarrow \bar{x}); \quad C'_0(x, \omega) = \frac{1}{Q^2} \frac{\ln(1 + \omega[\bar{x} - x])}{1 + \omega[\bar{x} - x]} + (x \rightarrow \bar{x}), \quad (\text{C.2})$$

and their convolutions with V_a and V_b , the latter being parts of the LO ERBL kernel,

$$V_a(y, x) = 2C_F \theta(x - y) \frac{y}{x} + (x \rightarrow \bar{x}, y \rightarrow \bar{y}); \quad V_b(y, x) = 2C_F \frac{y}{x} \frac{\theta(x - y)}{x - y} + (x \rightarrow \bar{x}, y \rightarrow \bar{y}); \quad (\text{C.3})$$

$$V_0(y, x) = V_a(y, x)_+ + V_b(y, x)_+ = 2C_F \left[\theta(x - y) \frac{y}{x} \left(1 + \frac{1}{x - y} \right) + (x \rightarrow \bar{x}, y \rightarrow \bar{y}) \right]_+. \quad (\text{C.4})$$

Here, the $_+$ -form of a distribution $V(y, x)$ is defined in the common way:

$$V(y, x)_+ \equiv V(y, x) - \delta(y - x) \int_0^1 V(u, x) du. \quad (\text{C.5})$$

The expression for diagram b) requires a more complicated construction involving K :

$$K(y, x) = C_F \theta(x - y) \frac{1}{x} - (x \rightarrow \bar{x}, y \rightarrow \bar{y}). \quad (\text{C.6})$$

The log terms, containing the ultraviolet scale μ_R^2 in Table C.1, are completely cancelled out on account of additional diagrams with self-energy corrections to the quark legs [8], with contributions of the form $\ln(\mu_F^2/\mu_R^2) \cdot C_0(x, \omega)$. The cancellation of the $\ln(\mu_R^2)$ terms for the full set of diagrams is a consequence of the Ward identity in QED. Finally, collecting the log terms from all diagrams, one obtains $\ln(\bar{Q}^2/\mu_F^2) \cdot C_0 \otimes V_0$ in accordance with Eq. (5).

To perform the (formal) limit $q^2 \rightarrow 0$ in (5), one has to take $\omega \rightarrow 1$ in the formulas of Table C.1, giving rise to the known expression for T_1 [8, 9], [16]:

$$T(Q^2, 0; \mu_F^2; x) = \frac{N_T}{Q^2} \left\{ \frac{1}{x} + \frac{\alpha_s(\mu_R^2)}{4\pi} \left[\ln \left(\frac{Q^2}{\mu_F^2} \right) \frac{1}{u} \otimes_u V_0(u, x) + \frac{C_F}{x} \left(\ln^2(x) - \frac{x \ln(x)}{1-x} - 9 \right) \right] \right\} \\ + (x \rightarrow \bar{x}) + \mathcal{O}\left(\frac{1}{Q^4}\right); \quad (\text{C.7})$$

$$C_1(Q^2, 0; x) = \frac{C_F}{xQ^2} \left(\ln^2(x) - \frac{x \ln(x)}{1-x} - 9 \right) + (x \rightarrow \bar{x}), \quad (\text{C.8})$$

At the scale $\mu_F^2 = \mu_R^2 = Q^2$, this leads to

$$\lim_{q^2 \rightarrow 0} Q^2 F^{\gamma^* \gamma \pi}(Q^2, q^2) = \sqrt{2} f_\pi \left(1 + \tilde{a}_2 + \tilde{a}_4 + \frac{\alpha_s(Q^2) C_F}{4\pi} [-5 + \tilde{a}_2 h_2 + \tilde{a}_4 h_4] - \frac{\delta(Q^2)}{Q^2} \frac{80}{27} \right); \quad (\text{C.9})$$

$$h_n \equiv \frac{1}{3} Q^2 C_1(Q^2, 0; x) \otimes_x \psi_n(x); \quad h_2 = \frac{295}{72}; \quad h_4 = \frac{10487}{900}, \quad (\text{C.10})$$

where $\tilde{a}_n = a_n^{\text{RG}}(Q^2)$ and h_n gives the size of the leading radiative corrections to the contribution of the n th Gegenbauer eigenfunctions $\psi_n(x)$, entering the expansion of $\varphi_\pi(x)$ (see Eq. (8)).

C.2 NLO coupling constant

Let us start with the RG equation for the (running) coupling constant in QCD:

$$\frac{da_s(Q^2)}{d\ln(Q^2)} = \beta(a_s(Q^2), N_f), \quad (\text{C.11})$$

where we put $a_s(Q^2) \equiv \alpha_s(Q^2) \left(\frac{b_0(N_f)}{4\pi} \right)$, N_f is the number of active flavors, and the corresponding β -function reads

$$\beta(a_s, N_f) = -a_s^2 [1 + c_1 a_s + c_2 a_s^2 + \dots], \quad (\text{C.12})$$

with $c_k \equiv c_k(N_f) = \frac{b_k(N_f)}{b_0(N_f)^{k+1}}$, and the standard β -function coefficients are given by

$$b_0(N_f) = \frac{11N_c - 2N_f}{3}; \quad (\text{C.13})$$

$$b_1(N_f) = \frac{34}{3}N_c^2 - \left(2C_F + \frac{10}{3}N_c\right)N_f; \quad (\text{C.14})$$

$$b_2(N_f) = \frac{2857}{2} - \frac{5033}{18}N_f + \frac{325}{54}N_f^2. \quad (\text{C.15})$$

Following here SY, we use the strong coupling constant in Sec. 3 in a ‘‘Particle Data Group’’ (PDG) form, which is the expanded second-order iteration of the 2-loop equation (C.11) (actually, it’s a 3-loop one due to appearing b_2 ??):

$$\alpha_s^{\text{PDG}}(Q^2, N_f) = \frac{4\pi}{b_0(N_f)L(Q^2)} \left[1 - \frac{L_1(Q^2)}{L(Q^2)} + \frac{L_1(Q^2)^2 - c_1 L_1(Q^2) - c_{12}}{L(Q^2)^2} \right] \quad (\text{C.16})$$

with

$$L(Q^2) \equiv \ln \left[\frac{Q^2}{\Lambda(N_f)^2} \right]; \quad L_1(Q^2) \equiv c_1 \ln(L(Q^2)); \quad c_{12} \equiv c_1^2 - c_2, \quad (\text{C.17})$$

where we fixed $\Lambda_5 = \Lambda(N_f = 5)$ with the help of [11]

$$\alpha_s(Q^2 = (91.2 \text{ GeV})^2, N_f = 5) = 0.118. \quad (\text{C.18})$$

Matching this coupling at the $N_f = 4$ threshold, $Q_4 = 10 \text{ GeV}$, and analogously at the $N_f = 3$ threshold, $Q_3 = 2.4 \text{ GeV}$, we arrive at

$$\Lambda_3 = 380 \text{ MeV}. \quad (\text{C.19})$$

But one can (we actually did this already in Sec. 4) use instead the exact solution of the 2-loop RG equation, rather than the PDG-booklet expression. This exact solution can be expressed in terms of the quantity a_s to read

$$\frac{1}{a_s(Q^2)} - c_1 \ln \left[\frac{1}{a_s(Q^2)} + c_1 \right] = L(Q^2). \quad (\text{C.20})$$

As has been shown in [28] the two-loop running coupling in QCD, being the solution of this equation, can be written via the Lambert W function:

$$\alpha_s^{2\text{-loop}}(Q^2, N_f) = -\frac{4\pi}{b_0(N_f)c_1} \left\{ 1 + W \left[-\frac{1}{c_1} \left(\frac{\Lambda^2(N_f)}{eQ^2} \right)^{1/c_1} \right] \right\}^{-1}. \quad (\text{C.21})$$

The difference between the PDG form and the exact solution varies from 3.5% at $Q^2 = 10 \text{ GeV}^2$ to 18% at $Q^2 = 1 \text{ GeV}^2$ when one uses the same value of $\Lambda = 380 \text{ MeV}$ for both functions. In a real situation, the values of Λ in the two cases are different and are fixed in accordance with the standard boundary condition (C.18), so that $\Lambda_3^{\text{PDG}} = 380 \text{ MeV}$ and $\Lambda_3^{2\text{-loop}} = 408 \text{ MeV}$. The deviation between the two forms becomes less pronounced at higher Q^2 and varies from 0.7% at $Q^2 = 10 \text{ GeV}^2$ to 10% at $Q^2 = 1 \text{ GeV}^2$ – see Fig. 5.

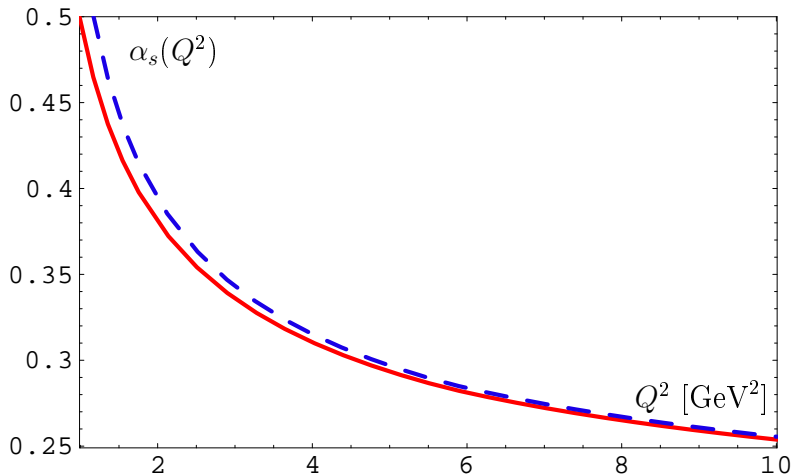


Figure 5: Q^2 -dependence of two different 2-loop running couplings, $\alpha_s^{2\text{-loop}}(Q^2)$ and $\alpha_s^{\text{PDG}}(Q^2)$: the solid line corresponds to the exact solution of the RG-equation, Eq. (C.21); the dashed line to the PDG-booklet approximate form, Eq. (C.16).

It should be realized from this comparison that the PDG formula (C.16) is afflicted by a large error at $Q^2 = 1 \text{ GeV}^2$ and for that reason it is preferable in the low Q^2 -region ($\leq 2 \text{ GeV}^2$) to use the exact formula (C.21). Only in the case of treating the heavy-quark thresholds in a more accurate way, as done in [29], the deviation between the PDG expression and the exact formula for the strong coupling starts to be insignificant even at $Q^2 = 1 \text{ GeV}^2$ (about 1.5%).

D The NLO evolution of DA

The ERBL evolution equation and its kernel have, respectively, the following structure (for more details, see, for example, [30])

$$\frac{\partial \varphi_\pi(x; \mu^2)}{\partial \ln \mu^2} = V(x, u; \alpha_s(\mu^2)) \otimes_u \varphi_\pi(x; \mu^2); \quad (\text{D.1})$$

$$V(x, u; \alpha_s) = \left(\frac{\alpha_s}{4\pi}\right) V_0(x, y) + \left(\frac{\alpha_s}{4\pi}\right)^2 V_1(x, y) + \dots \quad (\text{D.2})$$

Its eigenvalues $\gamma_n(\alpha_s)$ and eigenfunctions $\Psi_n(x; \alpha_s)$ are defined through

$$V(x, u; \alpha_s) \otimes_u \Psi_n(u; \alpha_s) = \gamma_n(\alpha_s) \Psi_n(u; \alpha_s). \quad (\text{D.3})$$

We use the following notations for its eigenvalues [31]

$$\gamma_n(\alpha_s) = \frac{-1}{2} \left[\left(\frac{\alpha_s}{4\pi}\right) \gamma_0(n) + \left(\frac{\alpha_s}{4\pi}\right)^2 \gamma_1(n) + \dots \right], \quad (\text{D.4})$$

where the coefficient 1/2 is due to historical reasons (when one defines evolution with respect to $\ln \mu$ instead of $\ln \mu^2$ this factor does not appear) and the sign “−” just allows one to work with

positive numbers $\gamma_0(n)$ and $\gamma_1(n)$ ⁹:

$$\gamma_0(0) = 0, \quad \gamma_1(0) = 0, \quad (\text{D.5})$$

$$\gamma_0(2) = \frac{100}{9}, \quad \gamma_1(2) = \frac{34450}{243} - \frac{830}{81}N_f, \quad (\text{D.6})$$

$$\gamma_0(4) = \frac{728}{45}, \quad \gamma_1(4) = \frac{662846}{3375} - \frac{31132}{2025}N_f. \quad (\text{D.7})$$

The two-loop eigenfunctions $\Psi_n^{2\text{-loop}}(x; \alpha_s)$ of the ERBL equation (D.1) can be expanded in terms of the one-loop eigenfunctions $\psi_n(x)$ (see Eq. (8)). The approximate solution (6) in NLO is then given by

$$\varphi_\pi^{\text{RG}}(x, \mu^2) = \sum_n a_n(\mu_0^2) \exp \left[\int_{a_s(\mu_0^2)}^{a_s(\mu^2)} \frac{\gamma_n(4\pi a/b_0) da}{\beta(a)} \right] \left[\psi_n(x) + \frac{\alpha_s(\mu)}{4\pi} \sum_{k>n} d_{nk}(\mu^2, \mu_0^2) \psi_k(x) \right] \quad (\text{D.8})$$

with $a_0 = 1$, see, e.g., [33]. The ‘‘diagonal’’ part (in the $\{\psi_n\}$ basis) of (D.8), expressed by the standard RG exponent, is the exact part of this solution, while the ‘‘non-diagonal’’ part is taken in the NLO approximation. The coefficients $d_{nk}(\mu^2, \mu_0^2)$, corresponding to the non-diagonal part, fix the mixing of the higher harmonics, $k > n$, due to the fact that the matrix of the anomalous dimensions is triangular in the $\{\psi_n\}$ basis. The exponent in (D.8) can be written explicitly (the scale μ_0^2 can be fixed at some arbitrary value $\simeq 1 \text{ GeV}^2$) to read

$$E(n, Q^2) \equiv \exp \left[\int_{a_s(\mu_0^2)}^{a_s(Q^2)} \frac{\gamma_n(4\pi a/b_0) da}{\beta(a)} \right] = \left[\frac{a_s(Q^2)}{a_s(\mu_0^2)} \right]^{\frac{\gamma_0(n)}{2b_0}} \left[\frac{1 + c_1 a_s(Q^2)}{1 + c_1 a_s(\mu_0^2)} \right]^{\omega(n)}, \quad (\text{D.9})$$

$$\omega(n) \equiv \frac{\gamma_1(n)b_0 - \gamma_0(n)b_1}{2b_0b_1}. \quad (\text{D.10})$$

Evolving according to (D.8), the Gegenbauer coefficients a_2, a_4 change from the scale $\mu_0^2 = \mu_{\text{SY}}^2$ ¹⁰ to the scale Q^2 as follows

$$a_2 \rightarrow U_2(Q^2, a_2) = a_2 E(2, Q^2) + \frac{\alpha_s(Q^2)}{4\pi} d_{02}(Q^2, \mu_0^2), \quad (\text{D.11})$$

$$a_4 \rightarrow U_4(Q^2, a_2, a_4) = a_4 E(4, Q^2) + \frac{\alpha_s(Q^2)}{4\pi} [d_{04}(Q^2, \mu_0^2) + a_2 E(2, Q^2) d_{24}(Q^2, \mu_0^2)] \quad (\text{D.12})$$

Here the NLO mixing coefficients are ($k = 2, 4 \geq n = 0, 2$)

$$d_{nk}(Q^2, \mu^2) = \frac{M_{nk}}{\gamma_0(k) - \gamma_0(n) - 2b_0} \left\{ 1 - \left[\frac{\alpha_s(Q^2)}{\alpha_s(\mu^2)} \right]^{\frac{[\gamma_0(k) - \gamma_0(n)]}{(2b_0) - 1}} \right\}, \quad (\text{D.13})$$

where the values of the first few elements of the matrix M_{nk} are

$$M_{02} = -11.2 + 1.73N_f, \quad M_{04} = -1.41 + 0.565N_f, \quad M_{24} = -22.0 + 1.65N_f. \quad (\text{D.14})$$

Analytic expressions for M_{nk} have been obtained in [32]. Using them one can estimate that the accuracy of (D.14) is of the order of 1%.

One appreciates from Eq. (D.8) that the NLO evolution inevitably generates higher harmonics. Even in our case, where we have as a starting point only two harmonics $a_2(\mu_0^2) \neq 0$ and $a_4(\mu_0^2) \neq 0$, the evolution to the scale Q^2 produces $a_k(Q^2) \neq 0$ for all $k \geq 6$. As one can see from Eq. (D.8), for $k \geq 6$ these harmonics are of NLO ($a_k(Q^2) \sim \alpha_s(Q^2)$). For this reason and owing to the enormous computational efforts needed for this task, we take into account only the complete NLO evolution of the first two nontrivial harmonics.

⁹This overall factor $(-1/2)$ in Eq.(D.4) is absent in Muller notations [32].

¹⁰Let us remind the reader that we use the values of a_2 and a_4 fixed at the scale $\mu_{\text{SY}}^2 = 5.76 \text{ GeV}^2$ as an input; this is done in order to facilitate comparison with the SY results.

E Main expressions for the NLO LCSR transition form factor

We employ a similar formalism as that used in [3, 2]. However, to make the present investigation self-contained, we provide explicit expressions, given also that the formulas provided in [2] are actually incomplete and only partially contained in [3]. All in all, the NLO LCSR transition form factor is

$$F_{\pi\gamma^*\gamma}(M^2, Q^2, a_2, a_4) = F_{\pi\gamma^*\gamma}^{\text{LO}}(M^2, Q^2, a_2, a_4) + \frac{\alpha_s(Q^2)C_F}{2\pi} F_{\pi\gamma^*\gamma}^{\text{NLO}}(M^2, Q^2, a_2, a_4) + F_{\pi\gamma^*\gamma}^{\text{TW-4}}(M^2, Q^2) \quad (\text{E.1})$$

with

$$F_{\pi\gamma^*\gamma}^{(\text{N})\text{LO}}(M^2, Q^2, a_2, a_4) = \quad (\text{E.2})$$

$$\frac{\sqrt{2}f_\pi}{3} \left[G_0^{(\text{N})\text{LO}}(Q^2, M^2) + U_2(Q^2, a_2)G_2^{(\text{N})\text{LO}}(Q^2, M^2) + U_4(Q^2, a_2, a_4)G_4^{(\text{N})\text{LO}}(Q^2, M^2) \right],$$

$$F_{\pi\gamma^*\gamma}^{\text{TW-4}}(M^2, Q^2) = \frac{\sqrt{2}f_\pi}{3} \left[\frac{1}{m_\rho^2} \int_0^{s_0} \rho^{\text{TW-4}}(Q^2, S) e^{\frac{m_\rho^2 - S}{M^2}} dS + \frac{1}{Q^2} H^{\text{TW-4}}(Q^2) \right], \quad (\text{E.3})$$

where the evolution functions $U_2(Q^2, a_2)$ and $U_4(Q^2, a_2, a_4)$ are described in Appendix D. We also define the following LCSR functions

$$Q^2 G_k^{\text{ORDER}}(Q^2, M^2) = \frac{Q^2}{m_\rho^2} \int_0^{s_0} \rho_k^{\text{ORDER}}(Q^2, S) e^{\frac{m_\rho^2 - S}{M^2}} dS + H_k^{\text{ORDER}}(Q^2); \quad (\text{E.4})$$

$$H_k^{\text{ORDER}}(Q^2) = \int_{s_0}^{\infty} \rho_k^{\text{ORDER}}(Q^2, S) \frac{Q^2 dS}{S}; \quad (\text{E.5})$$

$$H^{\text{TW-4}}(Q^2) = \int_{s_0}^{\infty} \rho^{\text{TW-4}}(Q^2, S) \frac{Q^2 dS}{S}, \quad (\text{E.6})$$

for $k = 0, 2, 4$ and set ORDER= LO or NLO. The spectral densities in LO are ¹¹

$$\rho_0^{\text{LO}}(u, s) = \frac{6us}{(u+s)^3}; \quad (\text{E.7})$$

$$\rho_2^{\text{LO}}(u, s) = \frac{36us(u^2 - 3us + s^2)}{(u+s)^5}; \quad (\text{E.8})$$

$$\rho_4^{\text{LO}}(u, s) = \frac{90us(u^4 - 10u^3s + 20u^2s^2 - 10us^3 + s^4)}{(u+s)^7} \quad (\text{E.9})$$

and in NLO (see [2]) —

$$\rho_0^{\text{NLO}}(u, s) = \frac{-us}{(u+s)^3} \left[15 - \pi^2 + 3 \left(\ln \frac{s}{u} \right)^2 \right]; \quad (\text{E.10})$$

$$\rho_2^{\text{NLO}}(u, s) = \frac{-s}{4(u+s)^5} \left\{ 25s^3 - 8(95 + 3\pi^2)s^2u + 36(25 + 2\pi^2)su^2 - 12(5 + 2\pi^2)u^3 + 12(s^2 - 3su + u^2)u \left(\ln \frac{s}{u} \right) \left[25 + 6 \ln \frac{s}{u} \right] \right\}; \quad (\text{E.11})$$

$$\rho_4^{\text{NLO}}(u, s) = \frac{-s}{10(u+s)^7} \left\{ 91s^5 - 2(5413 + 75\pi^2)s^4u + 125(541 + 12\pi^2)s^3u^2 - 100(901 + 30\pi^2)s^2u^3 + 150(193 + 10\pi^2)su^4 - 15(109 + 10\pi^2)u^5 + 30(s^4 - 10s^3u + 20s^2u^2 - 10su^3 + u^4)u \times \left(\ln \frac{s}{u} \right) \left[91 + 15 \ln \frac{s}{u} \right] \right\}. \quad (\text{E.12})$$

¹¹In the last part of this exposition, we use u instead of Q^2 in order to make the formulas more compact.

Contributions from higher states in LO are given by

$$H_0^{\text{LO}}(u) = \frac{3u^2}{(u+s_0)^2}; \quad (\text{E.13})$$

$$H_2^{\text{LO}}(u) = \frac{3u^2(u^2 - 8us_0 + 6s_0^2)}{(u+s_0)^4}; \quad (\text{E.14})$$

$$H_4^{\text{LO}}(u) = \frac{3u^2(u^4 - 24u^3s_0 + 90u^2s_0^2 - 80us_0^3 + 15s_0^4)}{(u+s_0)^6} \quad (\text{E.15})$$

and in NLO:

$$\begin{aligned} H_0^{\text{NLO}}(u) &= \frac{-15u^2}{2(u+s_0)^2} - \frac{3s_0}{(u+s_0)} \ln \frac{s_0}{u} + \frac{3(2u+s_0)s_0}{2(u+s_0)^2} \left[\left(\ln \frac{s_0}{u} \right)^2 - \frac{\pi^2}{3} \right] \\ &- 3 \left[\text{Li}_2 \left(-\frac{s_0}{u} \right) - \left(1 - \ln \frac{s_0}{u} \right) \ln \left(1 + \frac{s_0}{u} \right) \right]; \end{aligned} \quad (\text{E.16})$$

$$\begin{aligned} H_2^{\text{NLO}}(u) &= \frac{5u}{48(u+s_0)^4} (59u^3 - 352u^2s_0 + 564us_0^2 - 72s_0^3) \\ &+ \frac{3s_0}{2(u+s_0)^4} (12u^3 + 4us_0^2 + s_0^3) \left[\left(\ln \frac{s_0}{u} \right)^2 - \frac{\pi^2}{3} \right] \\ &+ \frac{1}{4(u+s_0)^4} (5u^4 + 4s_0(47u^3 - 3s_0(18u^2 + 3us_0 + s_0^2))) \ln \frac{s_0}{u} \\ &- 3 \left[\text{Li}_2 \left(-\frac{s_0}{u} \right) - \left(1 - \ln \frac{s_0}{u} \right) \ln \left(1 + \frac{s_0}{u} \right) \right] + \frac{5}{4} \ln \left(1 + \frac{u}{s_0} \right); \end{aligned} \quad (\text{E.17})$$

$$\begin{aligned} H_4^{\text{NLO}}(u) &= \frac{u}{600(u+s_0)^6} \left[10487u^5 - 149418u^4s_0 + 678285u^3s_0^2 - 888520u^2s_0^3 \right. \\ &\quad \left. + 259260us_0^4 - 6300s_0^5 \right] \\ &+ \frac{3s_0}{2(u+s_0)^6} (30u^5 - 75u^4s_0 + 100u^3s_0^2 + 6us_0^4 + s_0^5) \left[\left(\ln \frac{s_0}{u} \right)^2 - \frac{\pi^2}{3} \right] \\ &+ \frac{u}{10(u+s_0)^6} (44u^5 + 2124u^4s_0 - 7575u^3s_0^2 + 8000u^2s_0^3 \\ &\quad - 1425us_0^4 + 30s_0^5) \ln \frac{s_0}{u} - 3 \left(\ln \frac{s_0}{u} \right)^2 \\ &- 3 \left[\text{Li}_2 \left(-\frac{s_0}{u} \right) - \left(1 - \ln \frac{s_0}{u} \right) \ln \left(1 + \frac{s_0}{u} \right) \right] + \frac{7}{5} \ln \left(1 + \frac{u}{s_0} \right). \end{aligned} \quad (\text{E.18})$$

The twist-four spectral density is [3]

$$\rho^{\text{Tw-4}}(u, s) = \frac{80\delta^2(u)}{3u} \frac{2u^2s(s-u)}{(u+s)^5}, \quad (\text{E.19})$$

where $\delta^2(u)$ is taken from Eq. (A.4) with $\mu^2 = u$. This produces

$$H^{\text{Tw-4}}(u) = \frac{80\delta^2(u)}{3u} \frac{u^3(2s_0 - u)}{3(u+s_0)^4}. \quad (\text{E.20})$$

References

- [1] J. Gronberg *et al.*, Phys. Rev. **D57**, 33 (1998) [hep-ex/9707031].
- [2] A. Schmedding and O. Yakovlev, Phys. Rev. **D62**, 116002 (2000) [hep-ph/9905392].

- [3] A. Khodjamirian, Eur. Phys. J. **C6**, 477 (1999) [hep-ph/9712451].
- [4] A. V. Radyushkin and R. Ruskov, Nucl. Phys. **B481**, 625 (1996) [hep-ph/9603408].
- [5] A. P. Bakulev, S. V. Mikhailov, and N. G. Stefanis, Phys. Lett. **B508**, 279 (2001) [hep-ph/0103119]; in *Proceedings of the 36th Rencontres De Moriond On QCD And Hadronic Interactions, 17-24 Mar 2001, Les Arcs, France* [hep-ph/0104290].
- [6] A. P. Bakulev and S. V. Mikhailov, Phys. Rev. **D65**, 114511 (2002) [hep-ph/0203046].
- [7] A. V. Efremov and A. V. Radyushkin, Phys. Lett. **B94**, 245 (1980); Theor. Math. Phys. **42**, 97 (1980);
G. P. Lepage and S. J. Brodsky, Phys. Lett. **B87**, 359 (1979); Phys. Rev. **D22**, 2157 (1980).
- [8] F. del Aguila and M. K. Chase, Nucl. Phys. **B193**, 517 (1981);
E. Braaten, Phys. Rev. **D28**, 524 (1983).
- [9] E. P. Kadantseva, S. V. Mikhailov, and A. V. Radyushkin, Sov. J. Nucl. Phys. **44**, 326 (1986).
- [10] I. V. Musatov and A. V. Radyushkin, Phys. Rev. **D56**, 2713 (1997) [hep-ph/9702443].
- [11] D. E. Groom *et al.*, Eur. Phys. J. **C15**, 1 (2000).
- [12] V. M. Braun, A. Khodjamirian, and M. Maul, Phys. Rev. **D61**, 073004 (2000) [hep-ph/9907495].
- [13] V. L. Chernyak and A. R. Zhitnitsky, Phys. Rept. **112**, 173 (1984).
- [14] M. Diehl, P. Kroll and C. Vogt, Eur. Phys. J. **C22**, 439 (2001) [hep-ph/0108220].
- [15] A. Khodjamirian, Nucl. Phys. **B605**, 558 (2001) [hep-ph/0012271].
- [16] B. Melić, B. Nžić, and K. Passek, Phys. Rev. **D65**, 053020 (2002) [hep-ph/0107295].
- [17] S. Dalley and B. van de Sande, hep-ph/0212086.
- [18] S. V. Mikhailov and A. V. Radyushkin, Sov. J. Nucl. Phys. **49**, 494 (1989); Phys. Rev. **D45**, 1754 (1992);
A. P. Bakulev and S. V. Mikhailov, Phys. Lett. **B436**, 351 (1998).
- [19] V. A. Novikov, M. A. Shifman, A. I. Vainshtein, M. B. Voloshin, and V. I. Zakharov, Nucl. Phys. **B237**, 525 (1984).
- [20] A. A. Ovchinnikov and A. A. Pivovarov, Sov. J. Nucl. Phys. **48**, 721 (1988).
- [21] A. L. Kataev, G. Parente, and A. V. Sidorov, hep-ph/0106221 (unpublished).
- [22] V. M. Belyaev and B. L. Ioffe, Sov. Phys. JETP **57**, 716 (1983).
- [23] M. A. Shifman, A. I. Vainshtein, and V. I. Zakharov, Nucl. Phys. **B147**, 385, 448, 519 (1979).
- [24] B. L. Ioffe, hep-ph/0207191 (unpublished).
- [25] A. E. Dorokhov, S. V. Esaibegian, and S. V. Mikhailov, Phys. Rev. **D56**, 4062 (1997)
- [26] M. Praszalowicz and A. Rostworowski, Phys. Rev. **D64**, 074003 (2001) [hep-ph/0105188];
ibid. **D66**, 054002 (2002) [hep-ph/0111196].

- [27] V. L. Chernyak and A. R. Zhitnitsky, Nucl. Phys. **B201**, 492 (1982).
- [28] B. A. Magradze, in *Proceedings of the 10th International Seminar Quarks'98, Suzdal, Russia, 18–24 May 1998*, edited by F. L. Bezrukov *et al.* (INR RAS, Moscow, 1999), pp. 158–171 [hep-ph/9808247];
E. Gardi, G. Grunberg, and M. Karliner, JHEP **07**, 007 (1998) [hep-ph/9806462].
- [29] D. V. Shirkov and S. V. Mikhailov, Z. Phys. **C63**, 463 (1994) [hep-ph/9401270].
- [30] N. G. Stefanis, Eur. Phys. J. direct, **C7**, 1 (1999) [hep-ph/9911375]
- [31] F. J. Ynduráin, *Quantum Chromodynamics. An Introduction to the Theory of Quarks and Gluons*, (Springer-Verlag, New York, Berlin, Heidelberg, Tokyo, 1983), Eq. (20.12) and (21.10).
- [32] D. Müller, Phys. Rev. **D49**, 2525 (1994); *ibid.* **D51**, 3855 (1995).
- [33] S. V. Mikhailov and A. V. Radyushkin, Nucl. Phys. **B273**, 297 (1986).